4-17-2014

Observation of Coulomb repulsion between Cu intercalants in CuxBi2Se3

Chris Mann
University of Texas at Austin

Damien West
Rensselaer Polytechnic Institute

Ireneusz Miotkowski
Purdue University, irek@purdue.edu

Yong P. Chen
Purdue University, Birck Nanotechnology Center, yongchen@purdue.edu

Shengbai Zhang
Rensselaer Polytechnic Institute

See next page for additional authors

Authors
Chris Mann, Damien West, Ireneusz Miotkowski, Yong P. Chen, Shengbai Zhang, and Chih-Kang Shih

Observation of Coulomb repulsion between Cu intercalants in $Cu_xBi_2Se_3$

Chris Mann,[1] Damien West,[2] Ireneusz Miotkowski,[3] Yong P. Chen,[3,4] Shengbai Zhang,[2] and Chih-Kang Shih[1,5,*]

[1]*Materials Science & Engineering, University of Texas at Austin, Austin, Texas 78712, USA*

[2]*Department of Physics, Applied Physics, and Astronomy, Rensselaer Polytechnic Institute, Troy, New York 12180, USA*

[3]*Department of Physics, Purdue University, 525 Northwestern Ave., West Lafayette, Indiana 47907, USA*

[4]*Birck Nanotechnology Center and School of Electrical and Computer Engineering, Purdue University, West Lafayette, Indiana 47907, USA*

[5]*Department of Physics, University of Texas at Austin, Austin, Texas 78712, USA*

(Received 29 October 2013; revised manuscript received 1 April 2014; published 17 April 2014)

Using scanning tunneling microscopy and *ab initio* simulations, we have identified several configurations for Cu dopants in $Cu_xBi_2Se_3$, with Cu intercalants being the most abundant. Through statistical analysis, we show strong short-range repulsive interactions between Cu intercalants. At intermediate range (>5 nm), the pair distribution function shows oscillatory structure along the $\langle 10\bar{1}\rangle$ directions, which appear to be influenced by different diffusion barriers along the $\langle 10\bar{1}\rangle$ and $\langle 2\bar{1}\bar{1}\rangle$ directions.

DOI: 10.1103/PhysRevB.89.155312 PACS number(s): 68.37.Ef, 68.35.bg, 71.55.−i

I. INTRODUCTION

Understanding and controlling dopants in semiconductors has played a critical role in the development of modern semiconductor technology—the atomic configuration within the lattice and the electronic behavior of these (often) intentional impurities determines the type and quality of bulk electronic behavior [1–3]. While the advancement of materials synthesis techniques, such as molecular beam epitaxy, have been aimed at precise control of dopants with atomic-layer precision, including δ-doping schemes [4,5], several atomic-scale microscopy investigations have revealed rather complicated dopant distribution functions manifested by effective dopant-dopant interactions [6,7]. In the development of 3D topological insulators (TIs), understanding and controlling dopants is expected to play a similarly critical role in the materials advancement necessary to realize many predicted novel device properties. The behavior of dopants in 3D TIs, such as Bi_2Se_3, is inherently more complicated due to a significantly larger number of configurations available to dopants in these layered host materials. For instance, while many studies find that Cu is an *n*-type dopant in Bi_2Se_3, other studies have found that it can be used to prevent *n*-type doping—as an amphoteric defect, intercalated Cu is expected to *n*-dope the sample and Cu_{Bi} substitutions are expected to *p*-dope the sample [8]. While it has been found that heavily doped $Cu_xBi_2Se_3$ becomes superconducting [9–13], studies thus far have not distinguished where these Cu dopants physically reside in the Bi_2Se_3 samples. Other studies have found that strong band bending at the surface has limited Bi_2Se_3's viability as a TI, as the bulk conduction band is pulled down below the Fermi level and allows nontopological carriers [14–16]; attention has turned towards resolving these issues through clever doping schemes [17–19]. Therefore, understanding how Cu dopants are incorporated into the Bi_2Se_3 lattice is fundamental to understanding the consequences for the electronic structure and the surface state.

Here, we investigate the role of Cu with an atomic-scale resolution using scanning tunneling microscopy and *ab initio* simulations. We have characterized several Cu defects and, through comparison with simulation, determined their positions within the lattice. Statistical analysis of the spatial distribution of Cu shows that, when intercalated, Cu exhibits repulsive potentials characterized by a strong suppression of the pair distribution function at short separations. At longer range (>5 nm), the pair distribution function shows oscillatory structure along the $\langle 10\bar{1}\rangle$ directions that is absent along the $\langle 2\bar{1}\bar{1}\rangle$ directions.

II. EXPERIMENTAL DETAILS

Samples were grown using a Bridgman-type method similar to Mann *et al.* [20] and were prepared for analysis by cleaving in ultrahigh vacuum (UHV) at room temperature, then immediately transferred to the STM at 77 K. By cleaving the single-crystal samples, we are able to investigate the structure of the as-cleaved surface and near subsurface, the regime associated with topologically interesting behavior—we are unable to determine whether this is representative of the bulk structure. We observed ~500 pm nodules on the cleaved surface that we attribute to previously intercalated Cu that, upon cleaving, rearranged into clusters, shown in Fig. 1. The concentration of these nodules scales roughly linearly with the nominal bulk concentration of Cu, providing further evidence that these nodules are Cu clusters. All high resolution data was acquired in regions away from these large defects. Smaller defects with identifiable structure are visible in Figs. 2(a) and 2(b)—in addition to the nodules, we can identify five additional defects that are not observed in nominally undoped Bi_2Se_3, labeled defects A–E (only defects A–D are visible in Fig. 2).

Though Cu intercalants have long been expected to be the origin of *n*-doping in $Cu_xBi_2Se_3$ [8,10], a quantitative picture of the electronic interaction has not been developed, though their effect on strain has been noted [21]. We observed several Cu defects in $Cu_xBi_2Se_3$ with different topographic and tunneling signatures [Figs. 2(a)–2(d)], several of which have been observed by STM before (defects A–C) [11,22,23]; however, because STM lacks chemical specificity, we cannot definitively identify these defects without resorting to *ab initio* simulations of STM topographs. To simulate the Cu defects, we performed density functional theory calculations with single (7 × 7) quintuple-layer (QL) slabs using 98 Bi and

*Corresponding author: shih@physics.utexas.edu

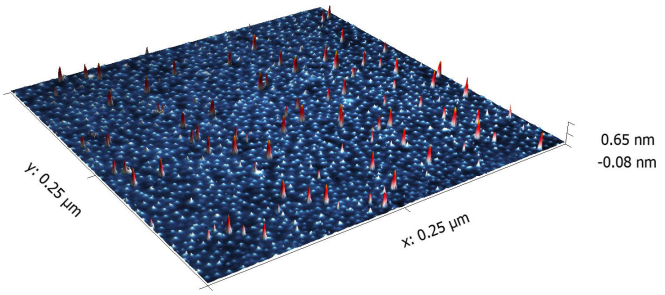

FIG. 1. (Color online) $Cu_{0.05}Bi_2Se_3$ after a room temperature cleave shows nodules on the surface. To prevent the tip from changing, we take data between these larger features. The nodule count appears to scale linearly with the nominal Cu doping level.

147 Se atoms; the technique is otherwise identical to that used in [20].

III. DEFECT IDENTIFICATION

Based on our simulations, defects B and C [Figs. 3(b) and 3(c)] are closest to the simulations of intercalants and appear with roughly equal concentration, though the simulations for the two defect sites (H and T) are qualitatively similar. In order to identify defect images observed via STM, we preformed *ab initio* density functional theory calculations.

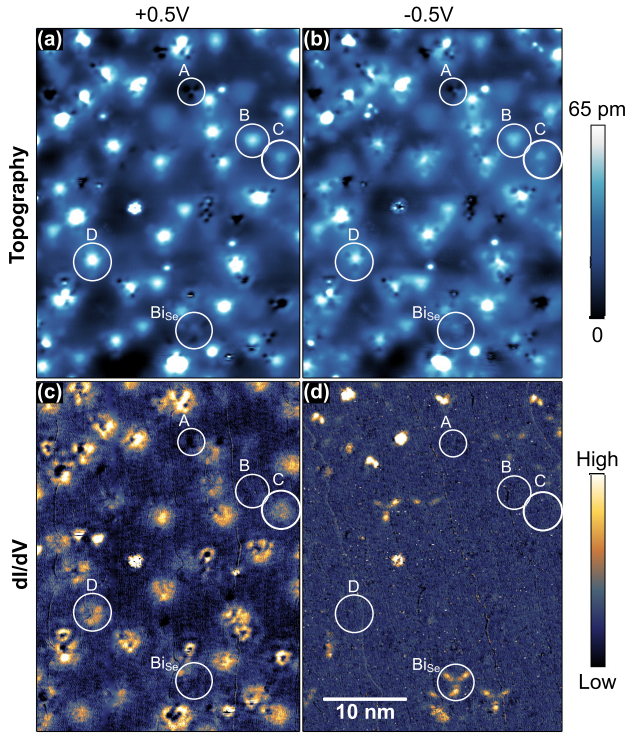

FIG. 2. (Color online) Topography (top) and dI/dV (bottom) at +0.5 V (left) and −0.5 V (right) of the same region of $Cu_{0.2}Bi_2Se_3$ at 500 pA. At −0.5 V, the Bi_{Se} antisite defects are weak features in the topography (c), though are prominent features in the dI/dV image (d). Additional defects are present, but are not well structured. They are likely multidefect complexes.

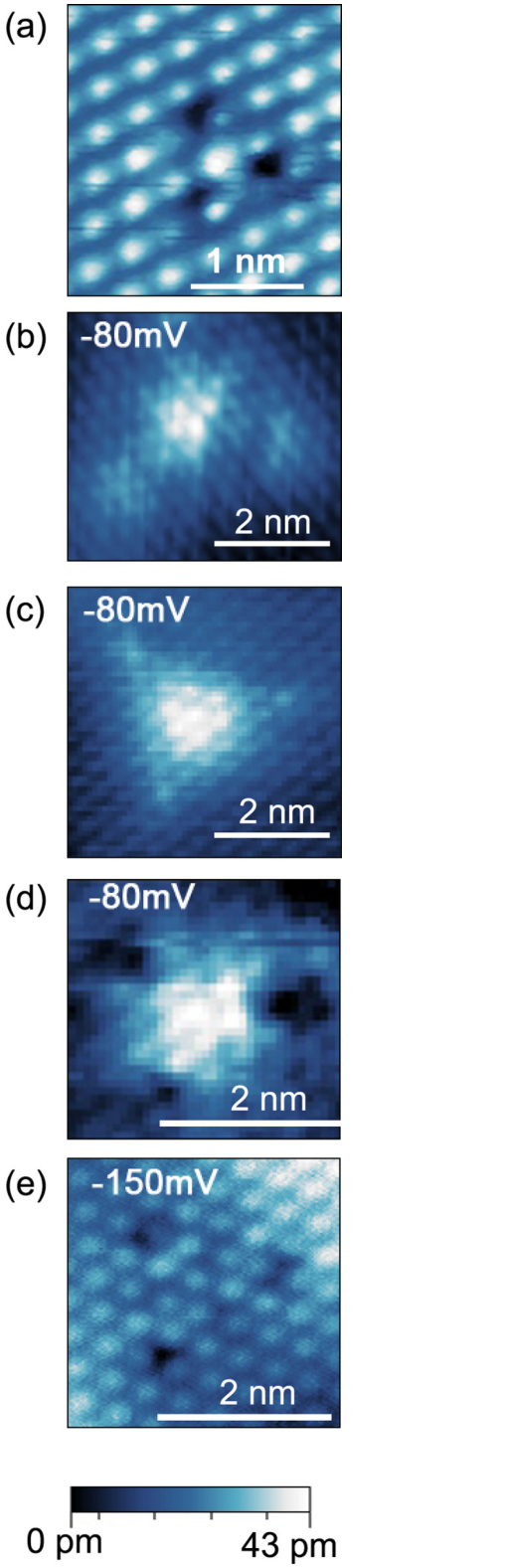

FIG. 3. (Color online) Detailed defect analysis. (a) Defect A atomic resolution topograph at 1 V, 480 pA. (b) Defect B topograph which we have associated with an H-site intercalant. (c) Defect C topograph which we have associated with a T4-site intercalant. (d) Newly identified defect D and (e) newly identified defect E. Color range for (e) is 18 pm; all others are 43 pm.

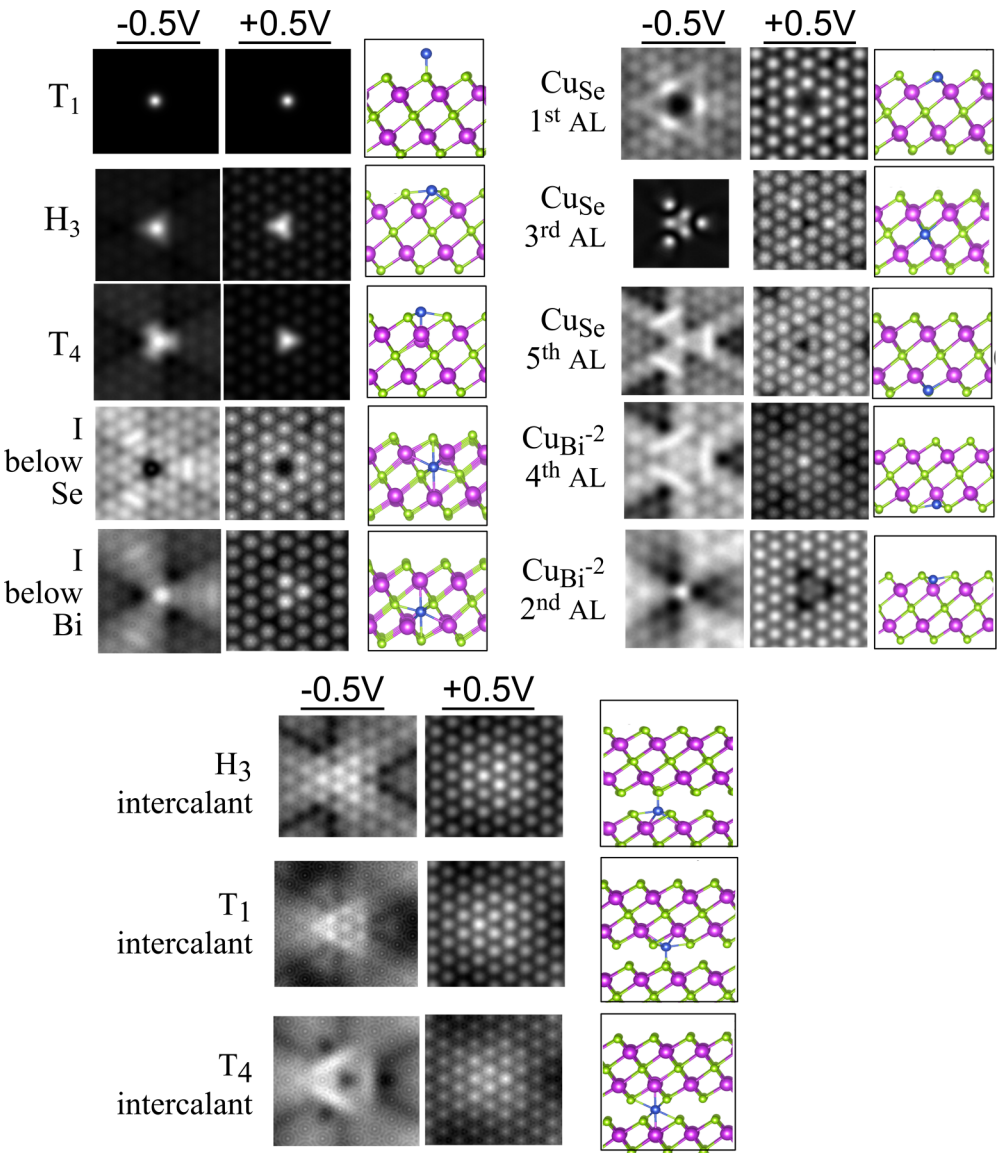

FIG. 4. (Color online) Simulated STM images for bias of −0.5 and +0.5 V for Fermi energy 0.3 eV above the CBM and corresponding defect structures. Cu_{Bi} in the second atomic layer is the closest match for defect A. Both Cu_{Se} (fifth layer) and Cu_{Bi} (fourth layer) have features common to defect D. Defects B and C are best associated with intercalant defects.

A number of Cu-related point defects were examined: substitutional Cu at the Bi and Se sites (Cu_{Bi} and Cu_{Se}), Cu adatom positions on the surface (T_1,H_3,T_4), interstitial Cu, and Cu intercalants in the van der Waals region. To adequately describe the interaction between slabs, dispersion forces were added using the DFT-D method [24,25]. The experimental Fermi energy is approximately 0.3 eV above the CBM, and the topological images are relatively insensitive to bias with the general features of defects A, B, C, and D yielding similar features for biases of −0.5 V and +0.5 V. Simulated images were calculated for each defect, according to the theory of Tersoff and Hamman [26] using the partial charge density from bands within a Fermi energy window between the CBM+0.3 eV and CBM+0.8 or −0.2 eV corresponding to positive and negative biases, respectively. The results are shown in Fig. 4. The T_4 adatom, interstitial Cu below Bi, and Cu_{Bi} in the second atomic layer all have features similar to defect A: a localized signature with a bright center and three dark spots. However, for positive bias only, Cu_{Bi} retains these features, making it the closest match in the currently considered defects. Similarly, the simulated images of Cu_{Se} in the fifth atomic layer as well as Cu_{Bi} in the fourth atomic layer share the same qualitative features of defect D, although at positive bias these features are much less prominent.

Defects B and C were the most widely observed defects in our samples and have been associated with intercalant defects; see Supplemental Material for more information about the defect counts [27]. Formation energy calculations support this, as the T_1, H_3, and T_4 intercalants were found to be the lowest energy Cu point defects in bulk. The larger features associated with these defects can be understood as the strain pushes the slabs apart leading to a slight bulging in the top quintuple slab, also consistent with the Cu intercalant assignment.

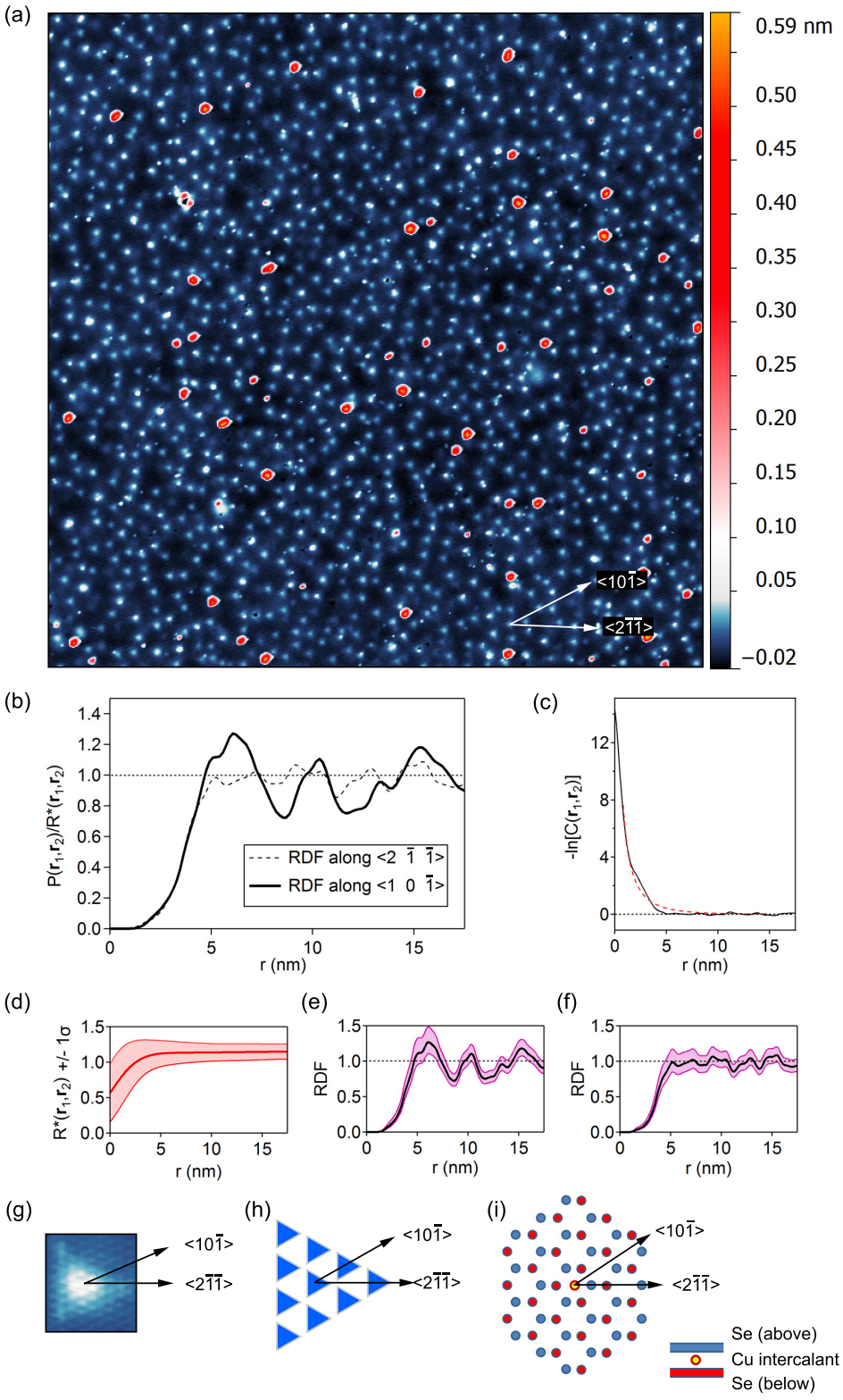

FIG. 5. (Color online) (a) 200 nm $\times$200 nm topography of nominally $Cu_{0.05}Bi_2Se_3$ showing 1020 Cu intercalants, white spots, and Cu clusters, red dots. (b) Radial distribution function of Cu intercalants extracted from (a) along directions of major symmetry. (c) A repulsive interaction is shown by the potential of mean force, determined by taking the log of the radial distribution function (solid line). The dotted line is a fit to the Yukawa potential; the screening length was found to be 3.9 ± 0.4 nm. The normalization factor was determined by computing the radial distribution function for an ensemble of random distributions and is plotted with its pointwise standard deviation in (d). To determine whether the structure within the radial distribution functions is within 1σ, we normalized the distribution functions along $\langle 10\bar{1} \rangle$ and $\langle 2\bar{1}\bar{1} \rangle$ by $R^*(\mathbf{r}_1,\mathbf{r}_2) \pm \sigma$, as shown in (e) and (f). The lattice vectors are plotted on top of a C-type defect (g). The observed structure indicates that the preferred ordering at this intercalant density is similar to that shown in (h). The observed directional anisotropy is attributed to diffusion barrier anisotropy: hopping along sites in the $\langle 10\bar{1} \rangle$ direction has a lower barrier than the $\langle 2\bar{1}\bar{1} \rangle$ direction, as shown by the lattice sites in (i).

IV. STATISTICAL ANALYSIS

Qualitatively, we noticed that the Cu intercalants are rarely found to be overlapping—they appear to maintain distance from each other, implying a repulsive interaction between intercalants. Quantitatively, this effect can be expressed by the pair distribution function, $P(\mathbf{r}_1,\mathbf{r}_2)$, the result of which is shown in Fig. 5(b), based on the analysis of 1020 intercalants (B and C type) in a 200 nm $\times$ 200 nm window [Fig. 5(a)]. Note that in this statistical analysis, we make a distinction between the pair distribution functions along two inequivalent directions, $\langle 10\bar{1} \rangle$ and $\langle 2\bar{1}\bar{1} \rangle$. Also shown in Fig. 5(d) is the random pair distribution, denoted $R^*(\mathbf{r}_1,\mathbf{r}_2)$, which is generated using the

results of 100 000 random ensembles, each with identical defect counts and box dimensions as the STM data, similar to Ref. [7]. The range of $\pm 1\sigma$ statistical fluctuations due to the finite ensemble size is shown as the shaded area. Because this data was acquired at 77 K, there is some residual drift that can produce uncertainty in the position of the defects. Therefore, the calculation uses a kernel density method with a Gaussian kernel width of 1 nm. Furthermore, the calculation assumes a continuum (not a lattice model), so any data points below separation of 0.5 nm are not meaningful. Nevertheless, the strong suppression of the pair distribution in short pair separation (<5 nm) is quite evident.

To interpret the origin of this suppression of pair distribution at short distance, we plot the pair correlation function, defined as the ratio of the actual distribution to the random distribution, $C(\mathbf{r}_1,\mathbf{r}_2) = P(\mathbf{r}_1,\mathbf{r}_2)/R^*(\mathbf{r}_1,\mathbf{r}_2)$, in logarithmic scale as $-\ln C(\mathbf{r}_1,\mathbf{r}_2)$ versus the pair separation [Fig. 5(c)]. The pair correlation function can be associated to the effective pair interaction potential as $w(\mathbf{r}_1,\mathbf{r}_2) = -k_B T \ln[C(\mathbf{r}_1,\mathbf{r}_2)]$. The functional form of the pair correlation function suggests that the pair interaction is of screened-Coulombic nature. The screened Coulomb potential (or often referred to as the Yukawa potential) has a functional form of $\varphi(r) \sim \frac{1}{r} e^{-\kappa r}$, which is plotted as the dashed curve with $\kappa = 0.25\ \mathrm{nm}^{-1}$, corresponding to a screening length of 3.9 ± 0.3 nm. As these intercalant Cu atoms are n-type dopants and should have a charge state of $+1$, it is not surprising that there is Coulomb interaction between them. Interestingly, this is in contrast to the surface Cu adatoms, which prefer to arrange into clusters. Because there is a strong near-surface band-bending field, the local Fermi level is n-shifted, making ionization unfavorable [14]; we have previously estimated this field to be ~150 meV/nm [20].

Note that the Fermi energy of this sample is roughly 0.3 eV above the conduction band minimum. With an effective mass of $0.15 m_o$ [10], one can deduce a Fermi wavelength of $\lambda_F \sim 5.5$ nm. For an electronic system, the screening length should be of the same order of magnitude as the Fermi wavelength. Thus a screening length of ~4 nm strongly suggests that the free carriers provide the screening of Coulomb interactions between intercalants. In addition to a clear signature of short-range repulsive interactions, one also observes an oscillatory structure in the pair correlation function along the $\langle 10\bar{1}\rangle$ directions (but not along the $\langle 2\bar{1}\bar{1}\rangle$ directions). To verify that this is not noise, we normalized the pair correlation functions by $R^*(\mathbf{r}_1,\mathbf{r}_2) \pm \sigma$, as shown in Figs. 5(e) and 5(f). The $\langle 10\bar{1}\rangle$ directions show additional structure to within $\pm\sigma$, while the $\langle 2\bar{1}\bar{1}\rangle$ directions do not.

V. CONSEQUENCES AND INTERPRETATION OF OSCILLATIONS IN $C(\mathbf{r}_1,\mathbf{r}_2)$

The observed oscillations of $C(\mathbf{r}_1,\mathbf{r}_2)$ along the $\langle 10\bar{1}\rangle$ directions raises some interesting questions and evokes comparison to dopants in other systems. This oscillatory phenomenon is fundamentally different from Friedel oscillation phenomena reported previously for adsorbates on metal surfaces [28,29]. For Friedel oscillations, the period should be half of the Fermi wavelength, while the observed period is a factor of 2 longer, which may suggest the existence of higher order correlations. On the other hand, the interaction of Cu intercalants with the host material may involve complications such as local deformation of the Bi_2Se_3 lattice and many other factors, making the effective interactions far more complicated than a simple Coulomb picture (except, perhaps, at very short range). Furthermore, it raises the question of the stability of dopants within the material; perhaps there is a maximum concentration of dopants that can be introduced without causing phase segregation or dopant relocation [30,31]. Similar effects are known in traditional semiconductors [32]. On the other hand, if one can enhance the ordering, then it could lead to a reduction in the electronic scattering, resulting in an improvement in the electronic properties [5,33].

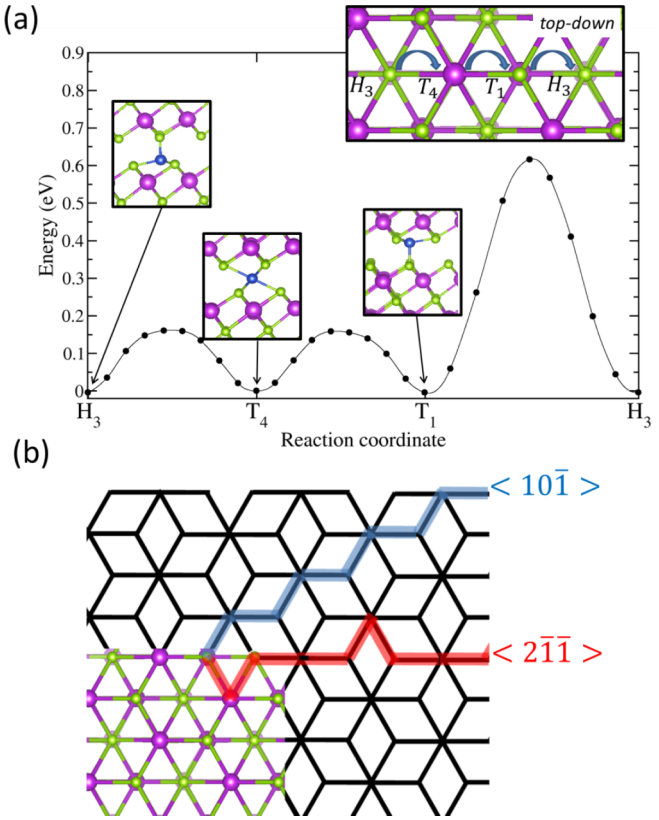

FIG. 6. (Color online) (a) Climbing image nudged elastic band calculation [34] of the kinetic barrier for diffusion of intercalated Cu directly in the $\langle 211\rangle$ direction. Eight images are chosen between each metastable minima, the energies of which are shown by the points. A spline is added between points as a guide to the eye. The small insets show the atomic structures at the H_3, T_4, and T_1 metastable configurations. The large inset is a top-down view depicting the successive hops taken into consideration in the calculation. (b) Schematic representation of the lattice where black lines are drawn between lattice registries which have a small barrier for Cu diffusion. Diffusion along the $\langle 10\bar{1}\rangle$ and $\langle 2\bar{1}\bar{1}\rangle$ directions are indicated by paths highlighted in blue and red, respectively.

In order to shed light on the observed differences in ordering along the $\langle 10\bar{1}\rangle$ and the $\langle 2\bar{1}\bar{1}\rangle$ directions, we investigated the mobility of intercalated Cu in the van der Waals gap. The three stable interstitial Cu positions were found to be nearly degenerate (within 5 meV) and are labeled according to the surface sites (T_1, T_4, and H_3) of the quintuple slab which lie directly *below* the intercalant Cu. The structures of these three configurations, as well as the kinetic barriers between them,

are shown in Fig. 6(a). Note that Cu above the T_1 site and H_3 sites are chemically identical, with Cu forming a vertical bond with the Se directly below or above it, respectively. However, direct hopping between these sites is found to be a high barrier process (0.63 eV), as Cu has to break and reform a number of bonds. On the other hand, diffusion to and from the T_4 site was found to be a low barrier process (0.16 eV), which, due to symmetry, is the same for both H_3 and T_1 sites.

Excluding high barrier processes, a schematic figure of the lattice is presented in Fig. 6(b), where the vertices correspond to atomic registries and the thick black lines correspond to allowed hops. Diffusion along either the $\langle 10\bar{1}\rangle$ or $\langle 2\bar{1}\bar{1}\rangle$ directions can be achieved through a series of low barrier hops, as indicated by the blue and red paths, respectively. However, it can be seen that the mobility along the $\langle 10\bar{1}\rangle$ direction is higher as diffusion can take place along a zigzag path with fewer hops required to achieve a greater displacement. Therefore, for any given number of hops, a greater response to the Coulombic repulsion can be achieved by responding along the $\langle 10\bar{1}\rangle$ direction, providing for a more structured distribution function in this direction.

VI. CONCLUSIONS

In summary, we have identified multiple Cu defects with STM and *ab initio* simulations of $Cu_xBi_2Se_3$. Our analysis of the radial distribution function has revealed that Cu intercalants physically repel each other with a screened Coulomb potential. The observed Coulombic repulsion may provide an opportunity for homogenizing the dopant distribution through self-ordering, as the ionized dopants within the van der Waals gap can reorganize to minimize their energy. But this observed mobility may also prove to be a challenging hindrance for some TI device applications where precisely positioned dopant profiles may relocate or reorganize, regardless of external design factors.

Note added. Additional defect counting information [35].

ACKNOWLEDGMENTS

C.M. and C-K.S. wish to acknowlege support from the Welch Foundation Grant No. F-1672, ARO Grants No. W911NF-09-1-0527 and No. W911NF-12-1-0308, and NSF Grant No. DMR-0955778. The work at Purdue was supported by the DARPA MESO program (Grant No. N66001-11-1-4107). D.W. acknowledges support of the Defense Award Research Project Agency (DARPA), Award No. N66001-12-1-4304, and S.B. acknowledges support of the US Department of Energy (DOE) under Grant No. DE-SC0002623. Supercomputer time was provided by NERSC under the Grant No. DE-AC02-05CH11231 and the Computational Center for Nanotechnology Innovations (CCNI) at RPI.

[1] J. Callaway and A. J. Hughes, Phys. Rev. **156**, 860 (1967).
[2] S. T. Pantelides, Rev. Mod. Phys. **50**, 797 (1978).
[3] H. J. Queisser and E. E. Haller, Science **281**, 945 (1998).
[4] K. Ploog, J. Cryst. Growth **81**, 304 (1987).
[5] A. F. J. Levi, S. L. McCall, and P. M. Platzman, Appl. Phys. Lett. **54**, 940 (1989).
[6] M. B. Johnson, P. M. Koenraad, W. C. van der Vleuten, H. W. M. Salemink, and J. H. Wolter, Phys. Rev. Lett. **75**, 1606 (1995).
[7] K.-J. Chao, C.-K. Shih, D. W. Gotthold, and B. G. Streetman, Phys. Rev. Lett. **79**, 4822 (1997).
[8] A. Vasko, L. Tichy, J. Horak, and J. Weissenstein, Appl. Phys. **5**, 217 (1974).
[9] N. Levy, T. Zhang, J. Ha, F. Sharifi, A. A. Talin, Y. Kuk, and J. A. Stroscio, Phys. Rev. Lett. **110**, 117001 (2013).
[10] L. A. Wray, S.-Y. Xu, Y. Xia, Y. S. Hor, D. Qian, A. V. Fedorov, H. Lin, A. Bansil, R. J. Cava, and M. Z. Hasan, Nat. Phys. **6**, 855 (2010).
[11] Y. S. Hor, A. J. Williams, J. G. Checkelsky, P. Roushan, J. Seo, Q. Xu, H. W. Zandbergen, A. Yazdani, N. P. Ong, and R. J. Cava, Phys. Rev. Lett. **104**, 057001 (2010).
[12] M. Kriener, K. Segawa, Z. Ren, S. Sasaki, and Y. Ando, Phys. Rev. Lett. **106**, 127004 (2011).
[13] T. Kirzhner, E. Lahoud, K. B. Chaska, Z. Salman, and A. Kanigel, Phys. Rev. B **86**, 064517 (2012).
[14] M. Bianchi, D. Guan, S. Bao, J. Mi, B. B. Iversen, P. D. C. King, and P. Hofmann, Nat. Commun. **1**, 128 (2010).
[15] M. Brahlek, Y. S. Kim, N. Bansal, E. Edrey, and S. Oh, Appl. Phys. Lett. **99**, 012109 (2011).
[16] I. A. Nechaev, R. C. Hatch, M. Bianchi, D. Guan, C. Friedrich, I. Aguilera, J. L. Mi, B. B. Iversen, S. Blugel, P. Hofmann, and E. V. Chulkov, Phys. Rev. B **87**, 121111 (2013).
[17] J. G. Analytis, R. D. McDonald, S. C. Riggs, J.-H. Chu, G. S. Boebinger, and I. R. Fisher, Nat. Phys. **6**, 960 (2010).
[18] Z. Ren, A. A. Taskin, S. Sasaki, K. Segawa, and Y. Ando, Phys. Rev. B **84**, 165311 (2011).
[19] S. S. Hong, J. J. Cha, D. Kong, and Y. Cui, Nat. Commun. **3**, 757 (2012).
[20] C. Mann, D. West, I. Miotkowski, Y. P. Chen, S. Zhang, and C.-K. Shih, Nat. Commun. **4**, 2277 (2013).
[21] C. Martin, V. Craciun, K. H. Miller, B. Uzakbaiuly, S. Buvaev, H. Berger, A. F. Hebard, and D. B. Tanner, Phys. Rev. B **87**, 201201 (2013).
[22] Y.-L. Wang, Y. Xu, Y.-P. Jiang, J.-W. Liu, C.-Z. Chang, M. Chen, Z. Li, C.-L. Song, L.-L. Wang, K. He, X. Chen, W.-H. Duan, Q.-K. Xue, and X.-C. Ma, Phys. Rev. B **84**, 075335 (2011).
[23] Z. J. Li, Y. Liu, S. C. White, P. Wahl, X. M. Xie, M. H. Jiang, and C. T. Lin, Phys. Procedia **36**, 638 (2012).
[24] S. Grimme, J. Comput. Chem. **27**, 1787 (2006).
[25] X. Wu, M. C. Vargas, S. Nayak, V. Lotrich, and G. Scoles, J. Chem. Phys. **115**, 8748 (2001).
[26] J. Tersoff and D. R. Hamann, Phys. Rev. B **31**, 805 (1985).
[27] See Supplemental Material at http://link.aps.org/supplemental/10.1103/PhysRevB.89.155312 for figure showing approximate defect counts and additional information about the statistical analysis.

[28] T. T. Tsong, Phys. Rev. Lett. **31**, 1207 (1973).
[29] J. Repp, F. Moresco, G. Meyer, K. H. Rieder, P. Hyldgaard, and M. Persson, Phys. Rev. Lett. **85**, 2981 (2000).
[30] E. F. Schubert, G. H. Gilmer, R. F. Kopf, and H. S. Luftman, Phys. Rev. B **46**, 15078 (1992).
[31] N. S. Averkiev, A. M. Monakhov, A. Shik, P. M. Koenraad, and J. H. Wolter, Phys. Rev. B **61**, 3033 (2000).
[32] P. Ebert, S. Landrock, Y. P. Chiu, U. Breuer, and R. E. Dunin-Borkowski, Appl. Phys. Lett. **101**, 192103 (2012).
[33] N. Kikegawa and K. Furuya, Physica B **227**, 57 (1996).
[34] G. Henkelman, B. P. Uberuaga, and H. Jónsson, J. Chem. Phys. **113**, 9901 (2000).
[35] This material is available free of charge via the Internet at http://pubs.acs.org.